Photodiode Response in a CH₃NH₃PbI₃/CH₃NH₃SnI₃ Heterojunction

Massimo Spina,[†] László Mihály,[‡] Károly Holczer,[§] Bálint Náfrádi,*[†] Andrea Pisoni,[†] László Forró,[†] and Endre Horváth[†]

[†]Laboratory of Physics of Complex Matter, Ecole Polytechnique Fédérale de Lausanne, CH-1015 Lausanne, Switzerland
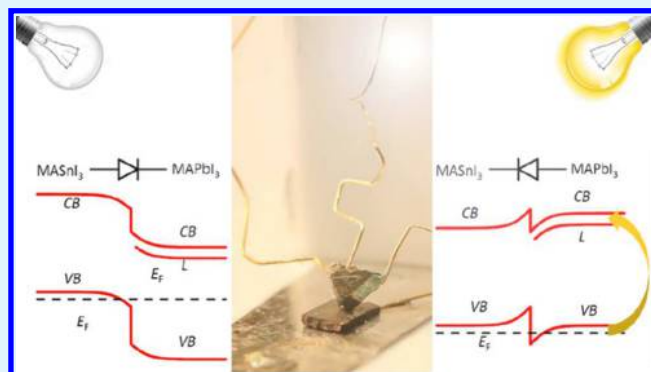[‡]Department of Physics and Astronomy, Stony Brook University, Stony Brook, New York 11790, United States
[§]Department of Physics and Astronomy, UCLA, Los Angeles, California 90095-1547, United States

Ⓢ *Supporting Information*

ABSTRACT: Here we report another surprising feature of the methylammonium metal halide material family, the photo-tunability of the diode response of a heterojunction made of CH₃NH₃PbI₃ and its close relative, CH₃NH₃SnI₃. In the dark state the device behaves as a diode, with the Sn homologue acting as the "*p*" side. The junction is extremely sensitive to illumination. A complete reversal of the diode polarity, the first observation of its kind, is seen when the junction is exposed to red laser light of 25 mW/cm² or larger power density. This finding opens up the possibility for a novel class of optoelectronic devices.

KEYWORDS: *photodiode, heterojunction, photovoltaics, photodetector, perovskite, methylammonium metal halide compounds*

INTRODUCTION

Since the discovery of its photovoltaic properties[2] organometallic salt CH₃NH₃PbI₃ became the subject of vivid interest. The material exhibits high light conversion efficiency,[3,4] it lazes in red color,[5] and it can serve as the basis for light emitting diodes[6] and photodetectors.[7−10] Also it shows unique properties for medical, thermoelectric, and data storage applications.[11−13] CH₃NH₃PbI₃ belongs to the family of methylammonium metal halide compounds, with the general composition of MA-MX₃, where MA stands for methylammonium, M is a metal ion (e.g., Pb²⁺, Sn²⁺) and X represents Cl⁻, Br⁻, I⁻, or F⁻.[14,15] The [MX₆]⁴⁻ octahedra are the building blocks of a perovskite structure. For the current study, large single crystals (MAPbI₃ 5−8 mm; MASnI₃ 1−2 mm in size), expressing cubelike or needle-shaped crystal habit, have been prepared by precipitation from a concentrated aqueous solution as described in ref 13 and the Supporting Information, section 1. Detailed characterization of materials are reported elsewhere.[9,13] To avoid sample degradation by moisture, the relative humidity at 23 °C temperature was fixed to 21%. The resistivity and the I−V characteristics of the materials have been studied separately in the dark state and also under illumination by white light and as a function of the temperature.[16] Representative I−V curves illustrating the photoresponse are shown in the Supporting Information, section 2. External quantum efficiency of the MAPbI₃−MASnI₃ junctions is characterized in the Supporting Information, section 4.

Junctions were prepared by touching a ~1 mm-size single crystal of MAPbI₃ to the surface of a freshly prepared MASnI₃ platelet. Electrical contacts were made by glued gold wires or tungsten pins pressed to the top of the MAPbI₃ crystal and to the MASnI₃ crystal close to the junction. A representative device is shown in Figure 1a. Owing to the presence of iodine vapor at the material's surface, the electrical contacts were susceptible to degradation with time, but the well-formed MAPbI₃−MASnI₃ junctions were stable. The I−V curves were obtained with a scan rate of 50 mV/s and a dwell time of 0.1 s, scanning from positive to negative voltages (i.e., from 0 to +1, then to −1, and back to 0 V). In order to minimize sources of external noise, the measurements were performed in a home-built Faraday cage. A microscope objective and a micro-mechanical stage were used to locate the device. We tested hundreds of such junctions and a subset of the devices—whose resistance was dominated by MAPbI₃−MASnI₃ interface—exhibited the behavior described below.

The diodelike rectifying behavior of the device is evident in the I−V characteristic (Figure 1b). In the forward bias regime (V < 0) the behavior looks nearly ohmic with a slope corresponding to 3 × 10⁹ Ω. Note that the resistance of the bulk MAPbI₃ component of the device falls in the same order of magnitude and it is very likely that in the forward bias regime the current-limiting factor is the ohmic resistance of the crystal. In the reverse bias direction we do not see a complete saturation of the current. This feature is contrary to the
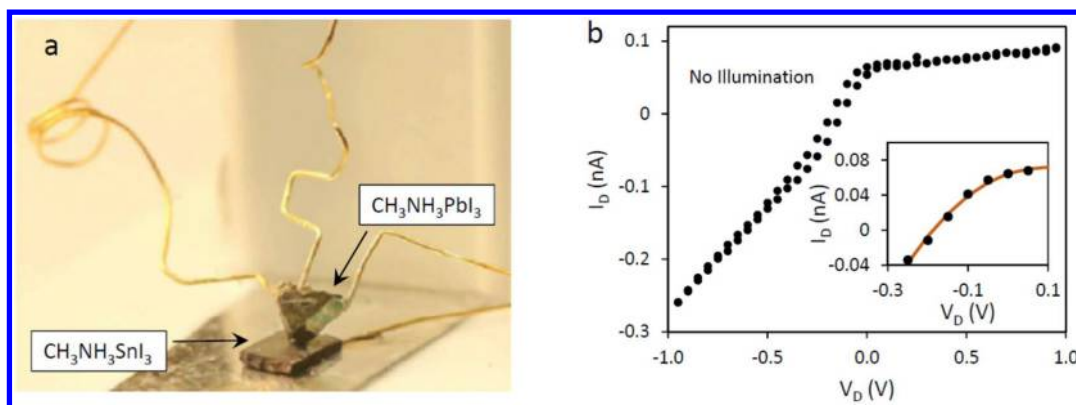
Figure 1. (a) Photograph of a photodiode similar to the ones used in this study. The MAPbI$_3$ bulk single crystal is mechanically compressed to a platelet of MASnI$_3$. Here the sample is contacted by gold wires, but most of the measurements were done in a two-probe configuration with tungsten pins pressed to the crystals. (b) Current−voltage characteristic of the diode in the dark state. (inset) Low-voltage behavior (dots) and a fit to a simple thermionic model (line). In the forward-biased region, the Sn homologue is the positive terminal.
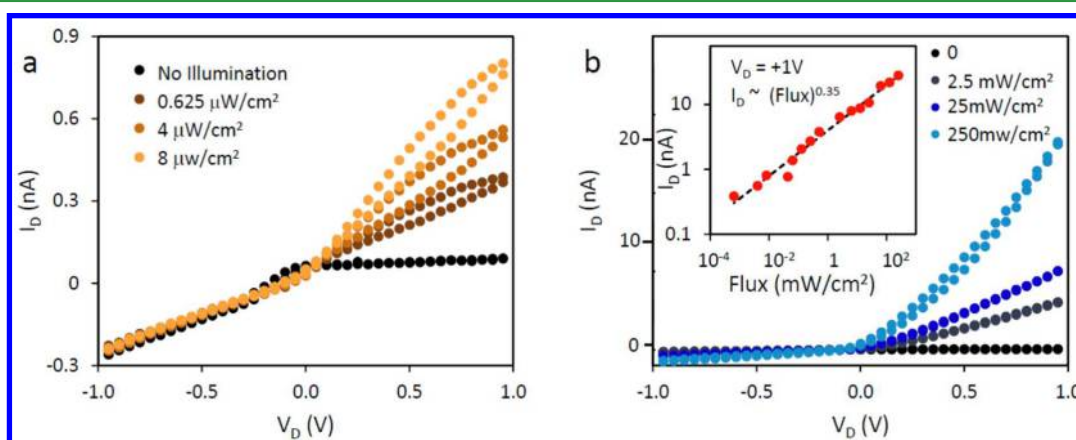

Figure 2. (a) Output characteristics of the photodiode at low light intensities (<10 μW/cm^2). Under illumination the lead compound starts conducting, and the I−V curve has an almost Ohmic shape with a hysteretic behavior for positive voltage. (b) Output characteristics of the photodiode for higher light intensities. The inset shows the current at the bias voltage of +1 V as the function of the light flux. The dashed line is a power−law fit.

behavior of a p−n junction or a heterojunction but consistent with a metal−semiconductor junction, where the reduction of the Schottky barrier by the image charges results in a voltage-dependent reverse current. The slope of the I−V curve corresponds to a resistance of 4×10^{10} Ω.

At zero current (open circuit) the device generates a voltage of $V_{OC} = 0.17$ V; at zero bias there is a short circuit current of $I_{SC} = 64$ pA. In these freshly made samples the surfaces are still chemically active. It is likely that there is a transfer of ions between the two sides of the junction, resulting in an electrochemical voltage generation. At zero bias this "battery voltage" drives the short circuit current.

In the low-bias regime, where the junction resistance is high, we may neglect the ohmic resistance of the bulk MAPbI$_3$ and we may model the junction with a simplified thermionic emission model.[17] The ideality factor (n) and the barrier height (U) of the junction has been evaluated (Supporting Information, section 3). The ideality factor, $n \geq 1$, gives the degree of the deviation of the diode characteristics from that of an ideal diode ($n = 1$). The red curve in the inset of Figure 1b represents a fit to the data yielding an ideality factor of $n = 9.7$. The large value of n indicates that the junction has inhomogeneities, probably related to the imperfect interface between the two materials. The same analysis yields a barrier

height of $U = 0.92$ eV. These values are reasonable, although the voltage range where the thermionic model works is rather limited.

The main finding reported here is the striking change in the behavior of the junction under illumination. Figure 2 shows the I−V curves of the device when the lead homologue is irradiated with red laser light ($\lambda = 633$ nm, spot size 4 mm^2). At low light intensities (i.e., < 5 μW/cm^2) reverse bias current evolves so that the junction becomes almost fully ohmic. As the voltage is scanned up and down, there is a hysteresis loop in the reverse biased region. With increasing light intensities (Figure 2b), the overall conductivity of the device increases dramatically, and at the same time there is a complete reversal of the forward and reverse bias behaviors. The ideality factor extrapolated for the device at different irradiation intensities varies between $n = 13$ and $n = 25$. The barrier height decreases approximately proportional with the light intensity reaching the value of 0.79 eV for 250 mW/cm^2.

We evaluated the photo response of the device as the function of incident light flux, as shown in the inset of Figure 2b. For positive bias of +1 V the current follows a power law dependence with an exponent of 0.35, for incident flux ranging from 0.625 to 250 mW/cm^2. There is no sign of saturation. The steady increase of current for nearly 6 orders of magnitude of

incident flux may be an extremely useful feature for light-sensing applications.

It is clear from the shape of the I−V curves in Figure 2 that the photoresponse of this device cannot be explained by the usual photoelectric effect, when electron−hole pairs created by the incident light carry a current through the device. Instead, we will use a model we proposed in an earlier study to explain the dramatic photoconductivity observed on the lead homologue.[16] The key element of the model is the introduction of a collection of narrow impurity states close to the conduction band. Charge carriers in this band are localized, but—in contrast to the usual doped semiconductors—in the dark state these states are unfilled and they can be attributed to charge neutral vacancies.[18] We have also postulated a hierarchy of relaxation rates (in particular a long relaxation rate from the impurity states to the valence band) that results in a "bottleneck" on the charge carrier's recombination path from the conduction band to the valence band.

Figure 3a illustrates the schematic band structure and the electron occupation in the ground state. We assume a flat form
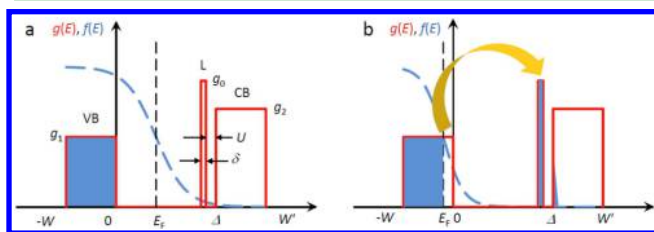

Figure 3. (a) Schematic density of states, $g(E)$, of MAPbI$_3$. The filled valence band (VB), the empty localized states (L), and the conduction band (CB) are indicated. The dashed line is the Fermi function $f(E)$, centered on the Fermi energy E_F. For a better view, the width of the Fermi function is exaggerated. (b) Electrons excited by light trapped in the localized states, causing a shift of the Fermi energy, as discussed in the text.

for the density of states $g(E)$, but the main features of the results will be the same for a more realistic functions. The Fermi energy is determined by the condition $N = V \int_{-W}^{W'} g(E)f(E) \, dE$, where N is the number of electrons and $-W$ and W' represents the bottom of the valence band and the top of the conduction band, respectively. Assuming that temperature is less than the bandwidths and the bandgap ($kT \ll \Delta, W$) and that the width of the localized band is much less than its separation from the conduction band ($U \ll \delta$), the Fermi energy is approximately determined by

$$0 = \int_{-W}^{W'} g(E)f(E) \, dE - \int_{-W}^{0} g(E) \, dE$$
$$= -g_1 kTe^{-E_F/kT} + g_2 kTe^{-\Delta-E_F/kT} + Ug_0 e^{-\Delta-\delta-E_F/kT}$$

For $g_1 = g_2$ and $g_0 = 0$, this yields the well-known result of $E_F = \Delta/2$ (independent of temperature). The unoccupied localized states push the Fermi level to a (temperature dependent) lower value. For example, if $g_1 kT = g_2 kT = Ug_0$, then $E_F = \Delta/2 - kT/2 \ln(1 + e^{\delta/kT})$.

Photoexcitation changes this picture drastically, due to the bottleneck effect described above. There will be a new dynamic equilibrium governed by the rates of excitation and the relaxation of the charge carriers, and the localized states will acquire a significant occupation. To illustrate the trends caused by this effect, we take the extreme case, when photoexcitation

nearly fills the localized states, as shown in Figure 3. The electrons trapped in the localized states leave behind an equal number of holes in the valence band. If thermal relaxation rates in the valence band are sufficiently high, the holes will thermalize around a new Fermi energy derived from $N - \delta N = V \int_{-W}^{W'} g(E)f(E) \, dE$, where δN is the number of trapped electrons. The result is illustrated in Figure 3.

Although here we assumed a narrow band of localized states, similar conclusions are achieved if the localized states are not separated by a gap δ from the conductions band, but instead the conduction band itself has a tail of localized states. Such states, separated from the delocalized states by the "mobility edge" has been widely discussed for disordered systems[19] and also for the materials used in the current study.[20,21]

The dramatic change of the Fermi energy in the photoexcited sample explains the reversal of the junction observed in the experiment, as illustrated in Figure 4. The Figure 4a shows the
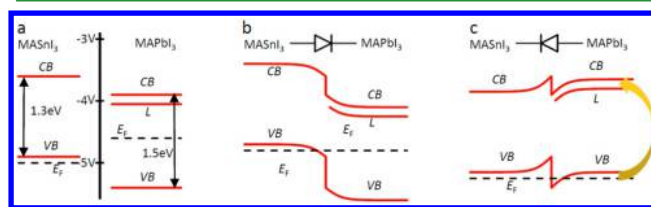

Figure 4. (a) Flat-band diagram of the two materials, based on band structure calculations.[1] The energies are relative to the vacuum energy. (b) Heterojunction formation in the dark state. (c) Electrons excited by light trapped in the localized states, causing a shift of the effective Fermi energy and a reversal of the junction.

flat-band energy diagram of the two materials, with an energy scale relative to the vacuum energy, based on band structure calculations.[1,22] Although structurally similar, MAPbI$_3$ and MASnI$_3$ have different electronic properties,[23,24] as reflected in the position of the Fermi energy. MAPbI$_3$ is an ambipolar semiconductor with a band gap of 1.5 eV, and the Fermi energy is approximately in the middle of the band gap. The resistivity of our MASnI$_3$ crystals vary between thermally activated (with an activation energy of 250 meV) and metallic, with a large range of room temperature resistances (10^3 to 10^{-3} Ω cm). Earlier studies demonstrated that this material can be easily doped to the metallic temperature dependence.[25] The variation in the properties of the MASnI$_3$ crystals can be attributed to the fact that the preparation involves the reduction of Sn^{IV} to Sn^{II} and a partial reduction results in a doped material.[21] For the current studies we selected a low resistance (highly doped) MASnI$_3$ crystal, and for those crystals the Fermi energy is near to the top of the valence band.

In the dark state the matching of the Fermi levels of MASnI$_3$ and MAPbI$_3$ yields a junction where the MASnI$_3$ is p-type relative to the MAPbI$_3$ (Figure 4b). When the photoexcitation shifts the Fermi level of the MAPbI$_3$, we have a p−P heterojunction, where the roles are switched and MAPbI$_3$ becomes the positive terminal of the diode. (Figure 4c).

The electrons trapped in the localized states cannot participate in the diffusion of charge carriers that typically happens when the heterojunction is formed. As a secondary effect, trapped localized charges in the interface region may also be responsible for the hysteresis seen in the low-bias I−V curves, shown in Figure 2a. The regular capacitive effects typical of a junction with a space-charge region result in a relatively

small capacitance, and this is not sufficient to explain the observed hysteresis at the low scanning rate used in our study. The response of the trapped charges can lead to a long-term memory in the junction, yielding to the observed behavior. In fact, the hysteresis is the subject of vivid interest in the field. Beyond the electronic trapping processes,[26] the ferroelectric domains[27,28] and the slow ion migration[29,30] are evoked as the source of the hysteresis. Whatever the origin of it, it is not the leading effect of this report.

CONCLUSION

In summary, we report a large photoresponse in a $CH_3NH_3PbI_3/CH_3NH_3SnI_3$ heterojunctions that steadily increasing with the incident flux for over more than 5 orders of magnitude of flux range. The behavior of the junction is different from the traditional photodiodes. In particular, the current in the junction is not carried by photoexcited electron hole pairs. Instead, under illumination we see a dramatic reversal of the diode's polarity. We propose an explanation based on a model where the incident light effectively induces an insulator to metal transition in the $CH_3NH_3PbI_3$ side of the junction. This is the very same model that has been used earlier to explain the photoresponse of the lead homologue.[16] We believe the unique properties described by the model are essential for this material's success in photovoltaic applications.

To our knowledge this is the first observation of such a dramatic reversal of polarity in a diode under illumination. Just like the first diodes (made of semiconductors and metal whiskers) or the first point-contact transistor made by Bardeen, Brattain, and Shockley,[31] our device is rudimentary, but it has the potential for novel applications, including the construction of extremely sensitive light sensors and other optoelectronic devices.

ASSOCIATED CONTENT

ⓈSupporting Information

The Supporting Information is available free of charge on the ACS Publications website at DOI: 10.1021/acsami.6b12392.

Sample preparation details, additional $I-V$ characterization, and calculation details (PDF)

AUTHOR INFORMATION

Corresponding Author

*E-mail: nafradi@yahoo.com.

ORCID ⓞ

Bálint Náfrádi: 0000-0001-9543-2970

Notes

The authors declare no competing financial interest.

ACKNOWLEDGMENTS

REFERENCES

(1) Wang, B.; Xiao, X.; Chen, T. Perovskite Photovoltaics: a High-efficiency Newcomer to the Solar Cell Family. *Nanoscale* **2014**, *6* (21), 12287−12297.

(2) Lee, M. M.; Teuscher, J.; Miyasaka, T.; Murakami, T. N.; Snaith, H. J. Efficient Hybrid Solar Cells Based on Meso-Superstructured Organometal Halide Perovskites. *Science* **2012**, *338* (6107), 643−647.

(3) Green, M. A.; Emery, K.; Hishikawa, Y.; Warta, W.; Dunlop, E. D. Solar Cell Efficiency Tables (Version 45). *Prog. Photovoltaics* **2015**, *23* (1), 1−9.

(4) Abrusci, A.; Stranks, S. D.; Docampo, P.; Yip, H. L.; Jen, A. K. Y.; Snaith, H. J. High-Performance Perovskite-Polymer Hybrid Solar Cells via Electronic Coupling with Fullerene Monolayers. *Nano Lett.* **2013**, *13* (7), 3124−3128.

(5) Xing, G. C.; Mathews, N.; Lim, S. S.; Yantara, N.; Liu, X. F.; Sabba, D.; Gratzel, M.; Mhaisalkar, S.; Sum, T. C. Low-temperature Solution-processed Wavelength-tunable Perovskites for Lasing. *Nat. Mater.* **2014**, *13* (5), 476−480.

(6) Tan, Z. K.; Moghaddam, R. S.; Lai, M. L.; Docampo, P.; Higler, R.; Deschler, F.; Price, M.; Sadhanala, A.; Pazos, L. M.; Credgington, D.; Hanusch, F.; Bein, T.; Snaith, H. J.; Friend, R. H. Bright Light-emitting Diodes Based on Organometal Halide Perovskite. *Nat. Nanotechnol.* **2014**, *9* (9), 687−692.

(7) Náfrádi, B.; Náfrádi, G.; Forró, L.; Horváth, E. Methylammonium Lead Iodide for Efficient X-ray Energy Conversion. *J. Phys. Chem. C* **2015**, *119* (45), 25204−25208.

(8) Spina, M.; Nafradi, B.; Tohati, H. M.; Kamaras, K.; Bonvin, E.; Gaal, R.; Forro, L.; Horvath, E. Ultrasensitive 1D field-effect Phototransistors: $CH_3NH_3PbI_3$ Nanowire Sensitized Individual Carbon Nanotubes. *Nanoscale* **2016**, *8* (9), 4888−4893.

(9) Horváth, E.; Spina, M.; Szekrényes, Z.; Kamarás, K.; Gaal, R.; Gachet, D.; Forró, L. Nanowires of Methylammonium Lead Iodide $(CH_3NH_3PbI_3)$ Prepared by Low Temperature Solution-Mediated Crystallization. *Nano Lett.* **2014**, *14* (12), 6761−6766.

(10) Spina, M.; Lehmann, M.; Náfrádi, B.; Bernard, L.; Bonvin, E.; Gaál, R.; Magrez, A.; Forró, L.; Horváth, E. Microengineered $CH_3NH_3PbI_3$ Nanowire/Graphene Phototransistor for Low-Intensity Light Detection at Room Temperature. *Small* **2015**, *11* (37), 4824−4828.

(11) Xu, W.; Cho, H.; Kim, Y.-H.; Kim, Y.-T.; Wolf, C.; Park, C.-G.; Lee, T.-W. Organometal Halide Perovskite Artificial Synapses. *Adv. Mater.* **2016**, *28* (28), 5916−5922.

(12) Náfrádi, B.; Szirmai, P.; Spina, M.; Lee, H.; Yazyev, O. V.; Arakcheeva, A.; Chernyshov, D.; Gibert, M.; Forró, L.; Horváth, E. Optically Switched Magnetism in Photovoltaic Perovskite $CH_3NH_3(Mn:Pb)I_3$. *Nat. Commun.* **2016**, *7*, 13406.

(13) Mettan, X.; Pisoni, R.; Matus, P.; Pisoni, A.; Jaćimović, J.; Náfrádi, B.; Spina, M.; Pavuna, D.; Forró, L.; Horváth, E. Tuning of the Thermoelectric Figure of Merit of $CH_3NH_3MI_3$ (M = Pb,Sn) Photovoltaic Perovskites. *J. Phys. Chem. C* **2015**, *119* (21), 11506−11510.

(14) Weber, D. $CH_3NH_3SnBrXI_{3-X}$ (X = 0−3) - SN(II)-System with Cubic Perovskite Structure. *Z. Naturforsch. (B)* **1978**, *33* (8), 862−865.

(15) Mitzi, D. B.; Wang, S.; Feild, C. A.; Chess, C. A.; Guloy, A. M. Conducting Layered Organic-inorganic Halides Containing < 110>;-Oriented Perovskite Sheets. *Science* **1995**, *267* (5203), 1473−1476.

(16) Pisoni, A.; Jacimovic, J.; Náfrádi, B.; Szirmai, P.; Spina, M.; Gaál, R.; Holczer, K.; Tutis, E.; Forró, L.; Horváth, E. Metallicity and Conductivity Crossover in White Light Illuminated $CH_3NH_3PbI_3$ Perovskite. *arXiv:1604.05637 [cond-mat.str-el]*, **2016**.

(17) Kim, J.; Lee, S.-H.; Lee, J. H.; Hong, K.-H. The Role of Intrinsic Defects in Methylammonium Lead Iodide Perovskite. *J. Phys. Chem. Lett.* **2014**, *5* (8), 1312−1317.

(18) Sze, S. M. *Physics of Semiconductor Devices*, 3rd ed.; John Wiley & Sons: New York, 1981.

(19) Anderson, P. W. Absence of Diffusion in Certain Random Lattices. *Phys. Rev.* **1958**, *109* (5), 1492−1505.

(20) Ma, J.; Wang, L.-W. Nanoscale Charge Localization Induced by Random Orientations of Organic Molecules in Hybrid Perovskite $CH_3NH_3PbI_3$. *Nano Lett.* **2015**, *15* (1), 248−253.

(21) La-o-vorakiat, C.; Salim, T.; Kadro, J.; Khuc, M. T.; Haselsberger, R.; Cheng, L.; Xia, H. X.; Gurzadyan, G. G.; Su, H. B.; Lam, Y. M.; Marcus, R. A.; Michel-Beyerle, M. E.; Chia, E. E. M. Elucidating the Role of Disorder and Free-carrier Recombination Kinetics in $CH_3NH_3PbI_3$ Perovskite Films. *Nat. Commun.* **2015**, *6*, 7.

(22) Umari, P.; Mosconi, E.; De Angelis, F. Relativistic GW Calculations on $CH_3NH_3PbI_3$ and $CH_3NH_3SnI_3$ Perovskites for Solar Cell Applications. *Sci. Rep.* **2014**, *4*, 4467.

(23) Takahashi, Y.; Obara, R.; Lin, Z.-Z.; Takahashi, Y.; Naito, T.; Inabe, T.; Ishibashi, S.; Terakura, K. Charge-transport in Tin-iodide Perovskite $CH_3NH_3SnI_3$: Origin of High Conductivity. *Dalton Transactions* **2011**, *40* (20), 5563−5568.

(24) Stoumpos, C. C.; Malliakas, C. D.; Kanatzidis, M. G. Semiconducting Tin and Lead Iodide Perovskites with Organic Cations: Phase Transitions, High Mobilities, and Near-Infrared Photoluminescent Properties. *Inorg. Chem.* **2013**, *52* (15), 9019−9038.

(25) Takahashi, Y.; Hasegawa, H.; Takahashi, Y.; Inabe, T. Hall Mobility in Tin Iodide Perovskite $CH_3NH_3SnI_3$: Evidence for a Doped Semiconductor. *J. Solid State Chem.* **2013**, *205*, 39−43.

(26) Shao, Y.; Xiao, Z.; Bi, C.; Yuan, Y.; Huang, J. Origin and Elimination of Photocurrent Hysteresis by Fullerene Passivation in $CH_3NH_3PbI_3$ Planar Heterojunction Solar Cells. *Nat. Commun.* **2014**, *5*, 5784.

(27) Wei, J.; Zhao, Y.; Li, H.; Li, G.; Pan, J.; Xu, D.; Zhao, Q.; Yu, D. Hysteresis Analysis Based on the Ferroelectric Effect in Hybrid Perovskite Solar Cells. *J. Phys. Chem. Lett.* **2014**, *5* (21), 3937−3945.

(28) Frost, J. M.; Butler, K. T.; Walsh, A. Molecular Ferroelectric Contributions to Anomalous Hysteresis in Hybrid Perovskite Solar Cells. *APL Mater.* **2014**, *2* (8), 081506.

(29) Richardson, G.; O'Kane, S. E. J.; Niemann, R. G.; Peltola, T. A.; Foster, J. M.; Cameron, P. J.; Walker, A. B. Can Slow-moving Ions Explain Hysteresis in the Current-voltage Curves of Perovskite Solar Cells? *Energy Environ. Sci.* **2016**, *9* (4), 1476−1485.

(30) Eames, C.; Frost, J. M.; Barnes, P. R. F.; O'Regan, B. C.; Walsh, A.; Islam, M. S. Ionic Transport in Hybrid Lead Iodide Perovskite Solar Cells. *Nat. Commun.* **2015**, *6*, 7497.

(31) PRESS RELEASE from Bell Telephone Laboratories, 463 Wast Street, New York, 14 CHelsea 3-1000 Release: A.M. Papers of Thursday July 1, 1948.